Resonant evanescent complex fields on dielectric multilayers

Resonant evanescent complex fields on dielectric multilayers

ANGELO ANGELINI[1*]

[1]*Department of Applied Science and Technology (DISAT), Politecnico di Torino, C.so Duca degli Abruzzi 24, 10129, Torino, Italy.*
**Corresponding author: angelo.angelini@polito.it*

Received XX Month XXXX; revised XX Month, XXXX; accepted XX Month XXXX; posted XX Month XXXX (Doc. ID XXXXX); published XX Month XXXX

Complex light fields including evanescent Bessel beams can be generated at dielectric interfaces by means of oil-immersion optics operating in total internal reflection conditions. Here, we report on the observation of evanescent complex fields produced on a dielectric multilayer through the interference of surface modes resonantly sustained by the multilayer itself. The coupling to surface modes is attained by modifying the wavefront of an incident laser beam in such a way that the resulting intensity distribution in k-space matches the dispersion of the surface mode. The phase of surface modes can be further controlled and two-dimensional vortex beams can be also produced, according to the same working principle.

OCIS codes: *(350.4238) Nanophotonics and photonic crystals; (240.6690) Surface waves; (230.5298) Photonic crystals;*

http://dx.doi.org/10.1364/OL.99.099999

The increasing capability of engineering light wave-fronts by combining holographic techniques with the use of resonant surface electromagnetic modes is enabling new tools in various fields such as optoelectronics, microscopy, nanofabrication or optical tweezing.[1-6] In this framework, the exploitation of Surface Plasmon Polaritons (SPPs) as near field energy carriers plays a relevant role because of the high degree of confinement of the electromagnetic field provided at the metal-dielectric interface and the possibility of manipulating the SPPs by nano-structuring the metallic surface.[7,8] In much simpler configurations, the direct coupling of tightly focused beams [9-11] or complex beams to SPPs through prisms or immersion optics has also been explored.[12-14] An evanescent Bessel beam is indeed characterized by a ring in its angular spectrum [15] and a non-diffractive behavior over a near field distance [11], and it has been already demonstrated that the natural wavevector filtering due to the resonant coupling condition may be exploited to produce evanescent Bessel beams [9,11,16-18].

Recently published works have demonstrated that one dimensional photonic crystals (1DPC) sustaining Bloch Surface Waves (BSWs) can be used as an alternative to metallic films sustaining SPPs to some extent [19-23]. An advantage of using photonic structures relies on the high Q-factors of the BSW resonances due to the low ohmic losses, especially in the visible range [24]. As an additional advantage, the multilayer structures can be tunable in terms of working wavelength (from UV to IR) and polarization response [25, 26].

Despite SPP and BSW rely on a different physics, the phenomenological analogy of these two effects is continuously inspiring new opportunities for replacing metallic thin films with dielectric multilayers [20,27].

Here we aim at exploiting BSWs to generate bi-dimensional complex optical fields with no need for surface nanostructures. More specifically, we employ a Spatial Light Modulator (SLM) to modify the wave-front of an incident laser beam in such a way that a controlled coupling of complex BSW field can occur through an oil-immersion objective.

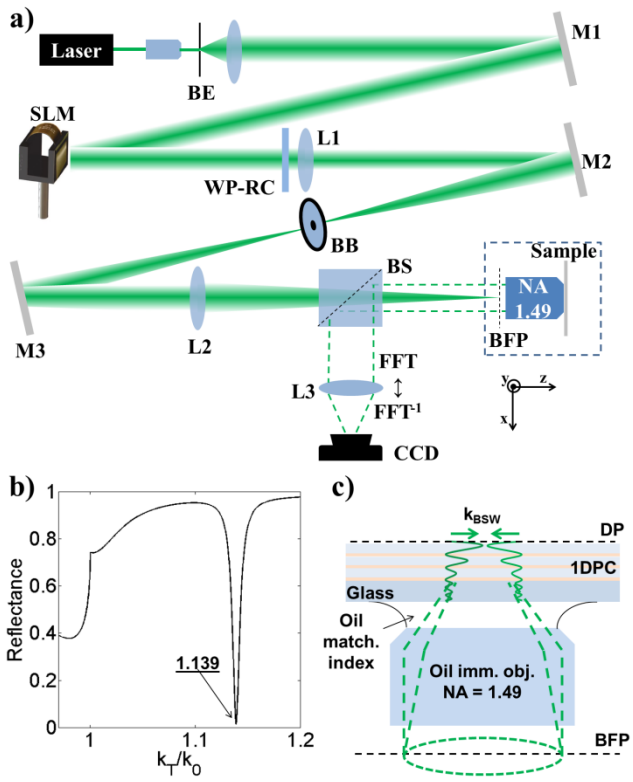

Fig. 1 a) Schematic view of the optical setup. b) s-polarized reflectivity profile calculated at λ = 532 nm as a function of the normalized transverse wave-vector component of an s-polarized plane wave incident on the multilayer from the glass side. c) Sketch of the sample stage with the oil-immersion objective oil-contacted to the glass substrate of the multilayer. The green dashed lines represent the laser beam path; the continuous green lines represent the electric field distribution of the BSW mode.

The experimental setup is sketched in fig. 1a. A linearly polarized TEM_{00} beam (CW frequency doubled Nd:Yag laser, wavelength λ = 532 nm and power 10 mW) is collimated by a beam expander (BE) constituted by a low Numerical Aperture (NA = 0.1) objective, a 50 μm pin-hole and a lens. The Gaussian beam coming out from the BE propagates toward the display of a phase only SLM (Holoeye PLUTO-VIS-016-C). The diameter of the beam is slightly larger than the display in order to maximize the SLM efficiency. The beam reflected by the SLM is Fourier-transformed by the lens L1. A beam blocker (BB) placed in the L1 focal plane can be used to filter out the zeroth-order. Subsequently, the laser beam can be eventually conditioned by using polarizing elements, e.g. a Quarter Wave Plate (QWP) or a Half Wave Plate (HWP). The lens L2 performs a 1:1 image formation of the BB place onto the Back Focal Plane (BFP) of an oil-immersion objective (NA = 1.49), which is oil-contacted to the glass substrate of the 1DPC.
Thanks to a beam splitter (BS), the light collected by the high NA objective can be imaged on a Charge Coupled Device (CCD) camera via a movable lens (L3). By changing the position of L3, either the BFP or the direct plane (DP) of the High NA objective can be imaged on the CCD.
The 1DPC structure is a multilayer having the following stack sequence: $(Ta_2O_5\text{-}SiO_2)$ x 4. The Ta_2O_5 layers are 70 nm thick (n_h = 2.08) while the SiO_2 layers are 210 nm thick (n_l = 1.45), with the exception of the last SiO_2 layer, which is only 180 nm thick. A more detailed description of the 1DPC employed here can be found in previous works [21,28]. The structure is designed to sustain TE polarized (s-polarized) BSWs in the visible range. Figure 1b shows a TE-polarized reflectance profile as function of the normalized transverse wave vector component $k_T/k_0 = n_{glass}\sin(\vartheta_{inc})$, where k_T is the transverse wave vector, i.e. the wavevector component parallel to the sample surface, and k_0 is the free-space wave vector of the incident radiation, n_{glass} = 1.5 is the glass substrate refractive index and ϑ_{inc} is the angle of incidence of a plane wave impinging on the 1DPC from the glass side. The profile, calculated at λ = 532 nm, shows a reflectance dip located at k_T/k_0 = 1.139 with a Full Width Half Maximum (FWHM) = 0.008. The appearance of the dip is associated to the resonant coupling of the free-space radiation to the BSW mode.
The SLM is used to shape the illumination beam incident on the 1DPC trough the oil-immersion objective. When the phase function of an axicon is generated on the SLM, a ring-shaped beam is projected in the BFP of the oil-immersion objective. The diameter of the ring can be adjusted by controlling the parameters of the Computer Generated Hologram (CGH) displayed on the SLM, meaning that we can adjust the transverse wave-vector components of the laser beam incident on the sample [29]. When the diameter of the ring projected in the BFP is such that the laser beam emerging from the oil-immersion objective contains a transverse wave-vector component equal to the BSW wave-vector, the light incident on the samples is partially reflected at the glass/1DPC interface and partially coupled to the BSW. The reflected light appears as a bright ring in BFP imaging, as showing in fig. 2a (the white arrow indicates the incident beam polarization). If the BSW coupling conditions are matched, the reflected light on the BFP image features a dark tiny arc corresponding to the reflectivity dip that one would obtain in Kretschmann configuration [21]. The dark arcs are oriented accordingly to the polarization of the incident beam in such a way that BSW coupling occurs in an s-polarized condition. In DP imaging, a large donut-shaped intensity distribution is collected, enclosing a complex pattern suggesting the presence of converging waves toward the optical axis (fig. 2b). It is well known that surface modes can be imaged through immersion optics by collecting the corresponding leakage radiation [30]. However, the large amount of reflected light may hinder the direct image of the surface mode. In order to overcome this effect, we slightly changed the position of the oil-immersion objective, in such a way that the leakage radiation only is collected (fig. 2c).
The BFP image in fig. 2c shows two bright narrow arcs with the same orientation of the dark arcs in fig. 2a. By switching to DP imaging (fig. 2d), we observe a magnified image of the central region of fig. 2b, from which the external bright donut shaped light is excluded. Fig. 2e and 2f are magnified views of portions (marked by the yellow dashed boxes) of the BFPs imaged respectively in fig. 2a and 2c. Figure 2g shows a comparison between the two vertical cross sections taken along the yellow dashed lines fig. 2e (black line) and 2f (red line). The black line profile shows a dip centered at k_y/k_0 = 1.135 ± 0.002 and a FWHM = 0.011 ± 0.004. The peak of the red line is centered at k_y/k_0 = 1.142 ± 0.002 and has a FWHM = 0.027 ± 0.004. The small displacement between the two peaks may be attributed to the slightly different magnification factor in the two BFP images. Additional uncertainty is due to the pixel sampling of the image. Such analysis confirms that the two BFP images are somehow complementary and that the dip observed in the reflected spot corresponds to surface propagating BSW-coupled radiation.
In the following, the DP imaging configuration will be considered, since it allows for directly image the surface distribution of light coupled to the BSW mode.

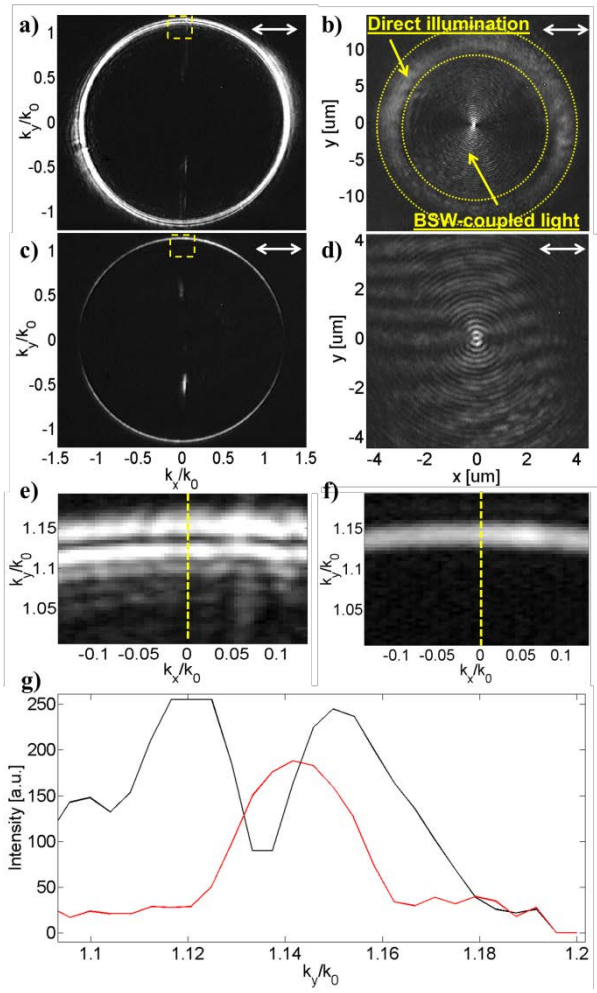

Fig. 2 a) Back Focal Plane image of the oil immersion objective showing the light reflected at the glass/1DPC interface. b) DP image corresponding to the BFP in a). c) BFP image showing the leakage radiation and in d) the corresponding DP image. e) and f) Zoom of the BFP region marked by the yellow dashed box respectively in a) and c). e) Intensity profiles taken along the yellow dashed lines in e) black line and in f) red line.

When a half-wave plate is introduced along the beam path, the beam polarization is rotated by 90°. By imaging the surface distribution of the leakage radiation, we can analyze the in-plane focusing features of the BSW coupled radiation. Figure 3a shows the spatial distribution of

the BSW coupled radiation at the air/1DPC interface when the incident beam is polarized along the *y*–axis (corresponding BFP in the inset). The radiation coupled to the BSW propagates along the air/1DPC interface, converging toward the center of the field of view, where a bright spot is produced. The fringes observable in the figures are caused by interference of the BSW-coupled radiation that is radially propagating on the surface. A similar focusing effect has been reported in a previous work, wherein a circular grating was used to couple converging BSWs [31]. The bright arcs in the BFP rotate accordingly to the polarization orientation (see inset in the figure), thus confirming the polarization dependence of the coupling mechanism. The polarization selectivity of the coupling mechanism would require therefore an azimuthal polarization of the incident beam in order to generate an effective Bessel beam distribution of the evanescent fields that would be characterized by a full ring in its angular distribution. [11,16]

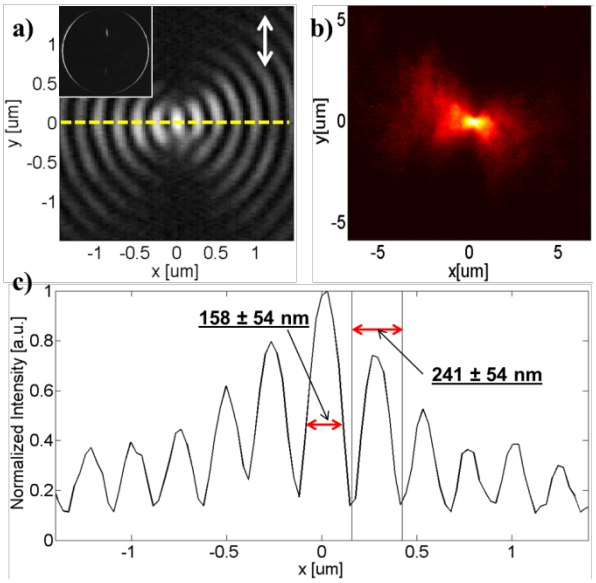

Fig. 3 a) DP images showing the laser intensity distribution on the surface of the 1DPC when the beam is linearly polarized along x. The electric field orientation is specified by the white arrow. In the inset the corresponding BFP image. b) Fluorescence image of the surface of the 1DPC. c) Intensity profile taken along the yellow dashed line in a).

As a further check of BSW coupling, we can observe the fluorescent trace of the laser BSW by covering the surface of the 1DPC with a homogenous fluorescent layer, in such a way that the fluorescent molecules act as near-field probes for the excitation field [10,21,24]. The image in fig. 3b confirms that the laser light is propagating along the surface and focusing in a diffraction limited spot. Unfortunately, the fluorescence image has an intrinsic limited resolution that does not allow a detailed analysis of the focal spot. Part of the fluorescence excited on the surface of the 1DPC couples in turn to the BSW and it is therefore delocalized on the surface [21,22,31]. An analysis of the intensity profile taken across the dashed yellow line in fig. 3a shows that the spot in the center has a FWHM = 158 ± 54 nm, while the periodicity of the fringes is estimated to be $P_{fringes}$ = 241 ± 54 nm, which is consistent with the theoretically predicted value of

$$\frac{\lambda}{2 * k_T/k_0} = 233\ nm$$

Here, the uncertainty of the estimation is mainly given by the discretization of the image introduced by limited pixel size of the CCD camera. It has to be pointed out here that both the periodicity of the fringes and the beamwidth of the focal spot are fixed for a given multilayer design, since both of them depend on the spatial frequency of the BSW.

When the incident beam is linearly polarized, the polarization-selective coupling of BSW limits the focusing effect along one direction. In order to overcome such a limitation, a QWP is introduced along the beam path so that a circularly polarized beam is obtained. Since the coupling occurs only for the s-polarized component of the incident beam, we expect that at each instant, only half of the donut shaped spot will have the correct polarization condition to be coupled to the BSW. By integrating the acquisition over a time much larger than a single period of rotation of the electric field, the intensity homogeneous leakage radiation ring observed in the fig. 4a is obtained. Since the CGH displayed on the SLM is azimuthally invariant (see inset in fig. 4a), each point of the ring generated is in phase with all the others. If the direct plane is imaged, the surface distribution of the BSW-coupled radiation confirms that at the center of the image a bright spot is generated, caused by constructive interference of all the converging BSWs (fig. 4b).

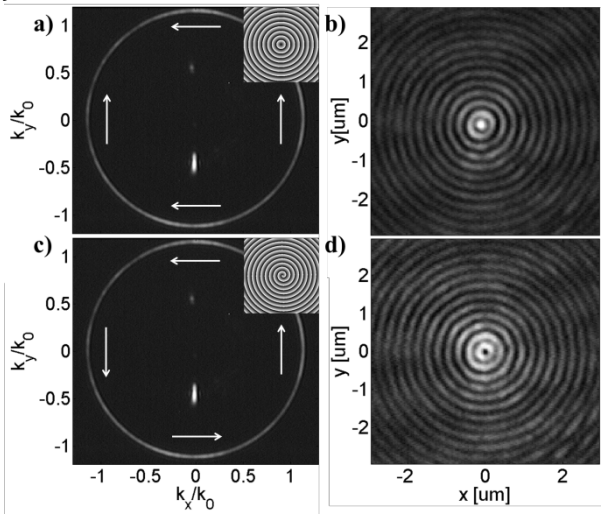

Fig. 4 a) Leakage BFP image for a circularly polarized Bessel beam. The white arrows show the orientation of the electric field. In the inset the CGH displayed on the SLM. b) DP image corresponding to the BFP in a). c) and d) are the same of a) and b) when the CGH in the inset in c) is displayed on the SLM.

By adding a continuous azimuthal phase delay to the CGH from 0 to 2π (see inset in fig. 4c), we can produce a spiral-like wavefront of the illumination beam (topological charge +1). The intensity distribution in the BFP does not vary (fig. 4c), but in this case at each time the opposite points have a relative phase difference of π (see the orientation of the white arrows in fig. 4c). The direct plane image clearly shows that the center of the interference pattern is now characterized by a dark hole, due to destructive interference along all the in-plane directions. It is worth to underline here that the switch between constructive and destructive interference has been obtained by software, with no need for changing anything in the optical setup or re-alignment.

In conclusion, this Letter shows that the resonant coupling of far-field radiation with near field surface modes combined with holographic techniques enables the generation of surface complex fields that can act as optical probes in different applications, from sensing to surface imaging. It has been shown that BSW-coupled radiation can be indeed confined in a tightly focused spot, and bi-dimensional optical vortices beams can be generated as well. One of the advantages of the proposed approach with respect to others proposed in literature is that it avoids the need for fabricating surface nanostructures to control the light propagation. The fabrication of nanostructures may be limiting in some applications, since it imposes a strong constrain over the localization of the optical fields on the surface, while the proposed approach may allow, for example, to scan the surface of the sample with the complex optical probe generated. Moreover, the use of SLM enables a dynamic control of the wave-front shape that is unfeasible with passive optical elements, which may be desirable in applications such as optical tweezing or surface nanofabrication.

Funding. Italian Flagship Project NANOMAX (Progetto Bandiera MIUR PNR 2011–2013).

Acknowledgment. The author gratefully thanks prof. Emiliano Descrovi for having inspired this work and for fruitful discussions. He also thanks Dr. Natascia De Leo (INRIM, Turin, Italy) and Dr. Peter Munzert (IOF, Jena, Germany) for technological support.

References

1. E. Ozbay, "Plasmonics: Merging Photonics and Electronics at Nanoscale Dimensions," Science **311**, 189 (2006).
2. K. J. Moh, X. C. Yuan, J. Bu, and B. Z. Gao, "Surface plasmon resonance imaging of cell-substrate contacts with radially polarized beams," Opt. Expr. **16**, 20734-41 (2008).
3. G. M. Lerman, A. Yanai, and U. Levy, "Demonstration of Nanofocusing by the use of Plasmonic Lens Illuminated with Radially Polarized Light," Nano Lett. **9**, 2139-43 (2009).
4. I. Dolev, I. Epstein and A. Arie, "Surface Plasmon holographic beam shaping," Phys. Rev. Lett. **109**, 203903 (2012).
5. C. Min et al., "Focused plasmonic trapping of metallic nanoparticles," Nat. Comm. **4**, 3891 (2013).
6. M. Righini et al., "Surface Plasmon Optical Tweezers: Tunable Optical Manipulation in the Femtonewton Range," Phys. Rev. Lett. **100**, 186804 (2008).
7. G. Rui, Q. Zhan and Y. Cui, "Tailoring optical complex field with spiral blade plasmonic vortex lens," Sci. Rep. **5**, 13732 (2015).
8. C. Zhao and J. Zhang, "Binary plasmonics: launching surface plasmon polaritons to a desired pattern," Opt. Lett. **34**, 2417-19 (2009).
9. Q. Zhan, "Evanescent Bessel beam generation via surface plasmon resonance excitation by a radially polarized beam," Opt. Lett. **31**, 1726-28 (2006).
10. G. Rui, Y. Lu, P. Wang, H. Ming, Q. Zhan, "Evanescent Bessel beam generation through filtering highly focused cylindrical vector beams with a defect mode one-dimensional photonic crystal," Opt. Comm. **283,** 2272–76 (2010).
11. W. Chen, Q. Zhan, "Realization of an evanescent Bessel beam via surface plasmon interference excited by a radially polarized beam," Opt. Lett. **34**, 722-24 (2009).
12. K. Kato, A. Ono, W. Inami, and Y. Kawata, "Plasmonic nanofocusing using a metal-coated axicon prism," Opt. Expr. **18,** 13580-85 (2010).
13. P. S. Tan et al., "Surface Plasmon polaritons generated by optical vortex beams," Appl. Phys. Lett. **92**, 111108 (2008).
14. K. Watanabe, G. Terakado, and H. Kano, "Localized surface plasmon microscope with an illumination system employing a radially polarized zeroth-order Bessel beam," Opt. Lett. **34**, 1180-82 (2009).
15. D. McGloin, K. Dholakia, "Bessel beams: diffraction in a new light," Cont. Phys. **46**, 15-28 (2005).
16. S. Ruschin, A. Leizer, "Evanescent Bessel beams," J. Opt. Soc. Am. A **15**, 1139-43 (1998).
17. W. B. Williams, J. B. Pendry, "Generating Bessel beams by use of localized modes," J. Opt. Soc. Am. A **22**, 992-97 (2005).
18. M. F. Imani, A. Grbic, "Generating Evanescent Bessel Beams Using Near-Field Plates," IEEE Trans. On Antennas and Propagation **60**, 3155-64 (2012).
19. E. Descrovi et al., "Guided Bloch Surface Waves on Ultrathin Polymeric Ridges," Nano Lett. **10**, 2087-91 (2010).
20. L. Yu et al., "Manipulating Bloch Surface Waves in 2D: a platform concept-based flat lens", Light: Sci. App. **3**, e124 (2014).
21. A. Angelini et al., "Fluorescence diffraction assisted by Bloch surface waves on a one-dimensional photonic crystal," New J. Phys. **15**, 073002 (2013).
22. R. Badugu, K. Nowaczyk, E. Descrovi, J. R. Lakowicz, "Radiative decay engineering 6: Fluorescence on one-dimensional photonic crystal," Anal. Biochem. **442**, 83-96 (2013).
23. M. Ballarini et al., "Bloch Surface Waves-controlled fluorescence emission: Coupling into nanometer-sized polymeric waveguides," Appl. Phys. Lett. **100**, 063305 (2012).
24. F. Michelotti et al., "Probing losses of dielectric multilayers by means of Bloch surface waves," Opt. Lett. **38**, 616-618 (2013).
25. R. D. Maede, K. D. Brommer, A. M. Rappe, and J. D. Joannopoulos, "Electromagnetic Bloch Waves at the surface of a photonic crystal," Phys. Rev. B **44**, 10961-64 (1991).
26. M. Liscidini, and J. E. Sipe, "Analysis of Bloch-surface-wave assisted diffraction-based biosensors," J. Opt. Soc. Am. B **26**, 279-289 (2009).
27. S. Ricciardi et al., "Optofluidic chip for surface wave based fluorescence sensing," Sens. Act. B **215**, 225-230 (2015).
28. A. Angelini et al., "In-plane 2D focusing of surface waves by ultrathin refractive structures," Opt. Lett. **39**, 6391-94 (2014).
29. A. Berrier, M. Swillo, N. Le Thomas, R. Houdré, and S. Anand, "Bloch mode excitation in two dimensional photonic crystals imaged by Fourier optics," Phys. Rev. B **79**, 165116 (2009).
30. E. Descrovi et al., "Leakage radiation interference microscopy," Opt. Lett. **38** (17), 3374-76 (2013).
31. A. Angelini et al., "Focusing and Extraction of Light mediated by Bloch Surface Waves", Sci. Rep. **4**, 5428 (2014).

References (abbreviated form)

1. E. Ozbay, Science **311**, 189 (2006).
2. K. J. Moh, X. C. Yuan, J. Bu, and B. Z. Gao, Opt. Expr. **16**, 20734-41 (2008).
3. G. M. Lerman, A. Yanai, and U. Levy, Nano Lett. **9**, 2139-43 (2009).
4. I. Dolev, I. Epstein and A. Arie, Phys. Rev. Lett. **109**, 203903 (2012).
5. C. Min et al., Nat. Comm. **4**, 3891 (2013).
6. M. Righini et al., Phys. Rev. Lett. **100**, 186804 (2008).
7. G. Rui, Q. Zhan and Y. Cui, Sci. Rep. **5**, 13732 (2015).
8. C. Zhao and J. Zhang, Opt. Lett. **34**, 2417-19 (2009).
9. Q. Zhan, Opt. Lett. **31**, 1726-28 (2006).
10. G. Rui, Y. Lu, P. Wang, H. Ming, Q. Zhan, Opt. Comm. **283,** 2272–76 (2010).
11. W. Chen, Q. Zhan, Opt. Lett. **34**, 722-24 (2009).
12. K. Kato, A. Ono, W. Inami, and Y. Kawata, Opt. Expr. **18,** 13580-85 (2010).
13. P. S. Tan et al., Appl. Phys. Lett. **92**, 111108 (2008).
14. K. Watanabe, G. Terakado, and H. Kano, Opt. Lett. **34**, 1180-82 (2009).
15. D. McGloin, K. Dholakia, Cont. Phys. **46**, 15-28 (2005).
16. S. Ruschin, A. Leizer, J. Opt. Soc. Am. A **15**, 1139-43 (1998).
17. W. B. Williams, J. B. Pendry, Opt. Soc. Am. A **22**, 992-97 (2005).
18. M. F. Imani, A. Grbic, IEEE Trans. On Antennas and Propagation **60**, 3155-64 (2012).
19. E. Descrovi et al., Nano Lett. **10**, 2087-91 (2010).
20. L. Yu et al., Light: Sci. App. **3**, e124 (2014).
21. A. Angelini et al., New J. Phys. **15**, 073002 (2013).
22. R. Badugu, K. Nowaczyk, E. Descrovi, J. R. Lakowicz, Anal. Biochem. **442**, 83-96 (2013).
23. M. Ballarini et al., Appl. Phys. Lett. **100**, 063305 (2012).
24. F. Michelotti et al., Opt. Lett. **38**, 616-618 (2013).
25. R. D. Maede, K. D. Brommer, A. M. Rappe, and J. D. Joannopoulos, Phys. Rev. B **44**, 10961-64 (1991).
26. M. Liscidini, and J. E. Sipe, J. Opt. Soc. Am. B **26**, 279-289 (2009).
27. S. Ricciardi et al., Sens. Act. B **215**, 225-230 (2015).
28. A. Angelini et al., Opt. Lett. **39**, 6391-94 (2014).
29. A. Berrier, M. Swillo, N. Le Thomas, R. Houdré, and S. Anand, Phys. Rev. B **79**, 165116 (2009).
30. E. Descrovi et al., Opt. Lett. **38** (17), 3374-76 (2013).
31. A. Angelini et al., Sci. Rep. **4**, 5428 (2014).